Sublattice site dependence of local electronic states in superstructures of CO built on a Cu(111) surface

Masashi Nantoh,[1,*] Kengo Takashima,[2] Takahiro Yamamoto,[2,3] and Koji Ishibashi[1,4]

[1]*Advanced Device Laboratory, RIKEN, Wako, Saitama 351-0198, Japan*
[2]*Department of Electrical Engineering, Tokyo University of Science, Katsushika, Tokyo 125-8585, Japan*
[3]*Department of Liberal Arts (Physics), Tokyo University of Science, Katsushika, Tokyo 125-8585, Japan*
[4]*RIKEN Center for Emergent Matter Science, Wako, Saitama 351-0198, Japan*

A two-dimensional electron gas interacting with an external periodic potential attracts attention as a designable artificial material to explore topological phases. Here, to introduce a periodic potential into a Shockley state, superstructures of CO molecules have been fabricated on a Cu(111) surface by atom manipulation with a low-temperature scanning tunneling microscope. Local electronic states have been investigated in relation to specific locations on the CO triangular lattice. All tunneling spectra of the lattice exhibit a reduction at the bottom energy of the surface-state band, which reflects absorption of surface-state electrons into the bulk. For an (8×8) CO structure, spectra measured at positions corresponding to two equivalent triangular sublattices of artificial graphene have different features near the Fermi level. This sublattice site dependence is not observed for a (6×6) structure. First-principles calculations for a (4×4) structure have reproduced the local density of states that depend on the sublattice sites. These results can be understood that coupling between the surface state and the bulk is strengthened via scattering by the adsorbates, and that the external periodic potential is perturbed by the second layer of the Cu(111) substrate. The periodicity of the external potential appears to be the key parameter which dominates the equivalence of pseudospin states in the artificial graphene.

I. INTRODUCTION

At the surface of a finite crystal, translational symmetry is broken in the normal direction. To minimize the total energy, a "real" surface relaxes or reconstructs the lattice of the topmost layers [1]. For an "ideal" surface, the translational invariance of the bulk is precisely retained in two dimensions, and the existence of surface states lying in forbidden energy gaps was predicted theoretically. Numerous following studies established two solutions of the surface states: a Shockley state using a nearly free electron model, and a Tamm state using a tight-binding model [2]. The band dispersions of these states have been reproduced with density functional theory (DFT) calculations employing slab geometries composed of five to ten atomic layers.

Cu(111) can be regarded as almost an ideal surface, and hence a good example to compare actual surface states with calculations [1]. The Shockley state, observed with angle-resolved photoemission spectroscopy, exhibits parabolic dispersion and a circular Fermi surface centered at the $\bar{\Gamma}$ point, reflecting the nearly free electron nature of the two-dimensional electron gas (2DEG) [3]. With scanning tunneling microscopy/spectroscopy (STM/STS), it has been visualized as standing waves near scatterers [4]. Because of the 2DEG, the Cu(111) surface is suitable for nanometer-scale atom manipulation experiments using low-temperature STM (LT-STM) [5]. The surface-state electrons can be confined within wall structures formed by adsorbates [6]. By means of controlling the shape and the size of the walls, it is possible to obtain tailored electronic structures [7,8].

Dirac materials, such as topological insulators [9] and graphene [10], have provided insight that a solid surface itself, or a monatomic layer on it, can be utilized as a functional material. Hence, these surfaces have attracted both scientific and technological interest. Moreover, it has been proposed that artificial Dirac fermion systems can be produced by fabricating nanometer-scale hexagonal potentials into conventional 2DEG's [11–13]. This has been realized in nanoscale-patterned semiconductors [14,15] and supramolecular networks on Cu(111) [16,17]. Furthermore, "molecular graphene," superstructures of CO molecules on Cu(111), have been used to create and control massless Dirac fermions, which allows inaccessible regimes of physical parameters in natural Dirac materials [18]. Accordingly, atom manipulation technique is a means to form artificial 2D electron systems that may bring valuable information to develop different functional materials.

Here, atom manipulation with LT-STM was used to fabricate small superstructures of CO molecules on a Cu(111) surface that correspond to "flakes of molecular graphene." STS was then performed to investigate their local density of states (LDOS). Figure 1 illustrates the $(N \times N)$ structure $(N = 8)$ that was fabricated, and indicates two equivalent locations for tunneling spectroscopy that correspond to two triangular sublattices (A and B) of a honeycomb lattice. The relationship between the LDOS at the A sublattice sites [LDOS(A)] and B sublattice sites [LDOS(B)] was examined. The surface state interacting with the periodic potential formed by the adsorbed molecules has the largest contribution to the LDOS spatial variation. The Shockley state can be regarded as isotropic in two dimensions because it is decoupled from the bulk state having threefold symmetry. The Cu(111) lattice and the CO superstructures, which are the primary source

*Corresponding author: nantoh@riken.jp
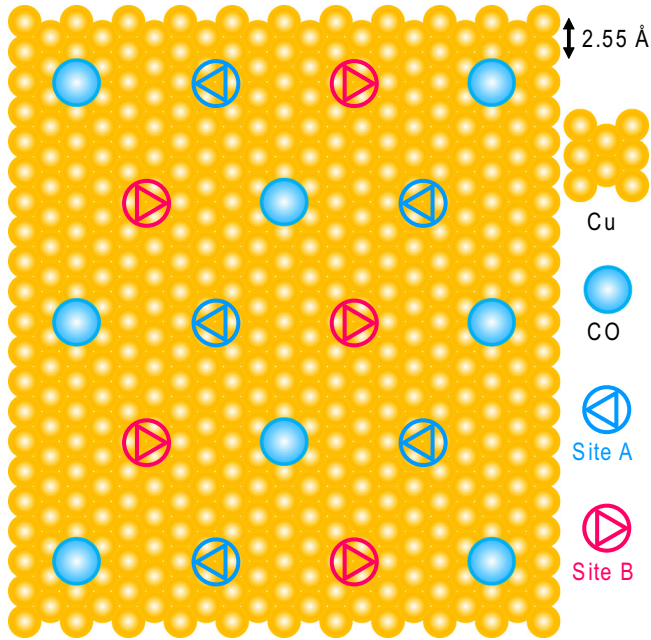
FIG. 1. Schematic of a $(N \times N)$ structure $(N = 8)$ of CO molecules on a Cu(111) surface and locations for spectroscopy measurements. Positions marked with open triangles having opposite orientations correspond to A and B sublattice sites in a honeycomb lattice (marked with open circles) of "molecular graphene."

FIG. 2. Tunneling spectroscopy on a CO-dosed Cu(111) surface. (a) STM image of randomly adsorbed CO molecules at low coverage shown in a contour display mode. Spectroscopy locations are indicated by numbered marks. The imaging conditions were $V_b = -0.2$ V, $I = 0.2$ nA, 20×20 nm^2, $T = 5.5$ K. (b) Tunneling spectra simultaneously obtained during the imaging scan at locations indicated in (a). The set point was $V_b = -2.0$ V, $I = 6.0$ nA, and the modulation for lock-in detection was $V_{AC} = 30$ mV, $f = 277$ Hz. Spectra 2–7 are offset vertically for clarity. Note that basic features in the spectra are independent of location.

of the potential, commonly have threefold symmetry and are commensurate. Therefore, the intuitional expectation was $\mathrm{LDOS}(A) = \mathrm{LDOS}(B)$. However, the experimental results indicated $\mathrm{LDOS}(A) = \mathrm{LDOS}(B)$ and $\mathrm{LDOS}(A) \neq \mathrm{LDOS}(B)$ depending on N, which was supported by the first-principles calculations. The possible origin and mechanism of this dependence are discussed.

II. EXPERIMENT

All experiments were performed with a homemade LT-STM operating at liquid helium temperatures ($\sim$4.2 K) in ultrahigh vacuum ($\sim$10^{-11} Torr). An electrochemically etched tungsten (W) wire was used for the STM tip. Image data were processed using WSxM v5.0 software (www.wsxmsolutions.com) [19]. Figure 2(a) and STS data are demonstrated in a contour display mode; other STM images shown below are in a derivative display mode.

The Cu(111) single crystal was cleaned by repeated cycles of sputtering with Ar$^+$ ions and annealing at 600 °C by electron bombardment. CO molecules were dosed on the sample surface when it was kept at <10 K to freeze molecular motion and isolate individual molecules. The CO coverage was controlled with a gas doser by counting voltage pulses of optimized duration to open an electromagnetic valve.

First-principles calculations were performed using a nonequilibrium Green's-function method combined with DFT [20]. The generalized gradient approximation in the Perdew-Burke-Ernzerhof parametrization (PBE-GGA) was used as the exchange-correlation functional, and the basis set was double-ζ polarized. A norm-conserving pseudopotential was used for all atoms. The real-space grid cutoff was 75 hartree,

and a 9×100 k-point mesh was used for the self-consistent calculations.

III. RESULTS AND DISCUSSION

Figure 2 shows STM/STS for CO molecules on the Cu(111) surface. CO molecules occupy on-top sites of the Cu(111) triangular lattice in an upright geometry with C atoms bonding to Cu. CO dimers are hardly formed due to the short-range repulsive intermolecular dipole-dipole interaction [21]. In the STM image [Fig. 2(a)], CO appears as dark depressions, which was commonly observed and theoretically explained [22–24]. If the STM tip had picked up a CO molecule at its apex, there would have been a contrast inversion from the depressions to protrusions [22]; this was not observed. However, it is likely that the W tip was covered with Cu after poking it into the substrate many times. Consequently, Cu $3d_{z^2}$ and $4s\,p_z$ orbitals of the tip seemed to contribute dominantly to the STM tunneling [25].

Figure 2(b) reveals tunneling spectra acquired during the imaging scan. The measurement locations are marked and labeled in Fig. 2(a). All the spectra have basically the same shape, independent of location. The main features are a large peak of the Cu $3d$ band located at around sample bias voltage $V_b = -2$ V, and an abrupt increase at about $V_b = -0.4$ V that corresponds to the bottom of the Shockley state [3]. Other characteristic peaks or dips that sometimes appear below the Fermi level (E_F) are attributed to resonance states caused by adsorbates on the tip [26] and are excluded here from consideration. The chemisorption of CO on Cu(111) is described by the Blyholder model [27] in terms of charge donation from the occupied CO 5σ orbital to the Cu states, and back donation from the Cu states to the unoccupied CO
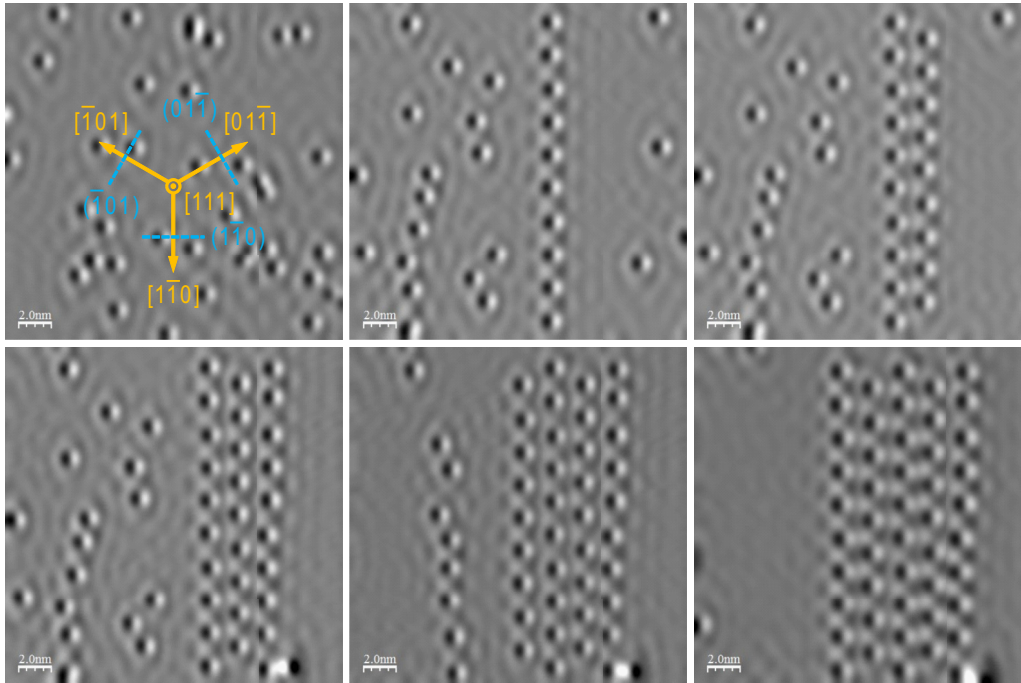
FIG. 3. Formation of a (8×8) CO structure on Cu(111) using atom manipulation. The STM images are shown in a derivative display mode. An artificial triangular lattice was fabricated by dragging molecules with the STM tip. The imaging conditions were $V_b = -0.2$ V, $I = 0.2$ nA, 20×20 nm^2, $T = 5.5$ K. For manipulation, $V_b = -0.01$ V, $I = 90$–150 nA. Here, 48 CO molecules were periodically arranged with a lattice spacing of 20.4 Å.

$2\pi^*$ orbital [28–31]. Because the large 5σ peak is located deeper than the binding energy of -6 eV, CO adsorption does not significantly change the spectral shape within the range $|V_b| < 1$ V.

Figure 3 demonstrates the fabrication of an (8×8) superstructure of 48 CO molecules with a lattice spacing of 20.4 Å. Manipulation of the CO molecules was achieved by dragging them with the STM tip at $V_b = -0.01$ V and tunneling current $I = 30$–150 nA, using homemade software. On the clean Cu(111) surface, the corrugation of the Cu atoms is too small for atomic resolution under normal imaging conditions. However, the [1$\bar{1}$0] and two equivalent directions of the Cu(111) triangular lattice are easily identified by finding three equivalent directions of straight steps rotated by 120° with respect to each other. When the atom manipulation experiments were performed, the y direction of the image was set parallel to one of these directions by adjusting the scanning angle. The CO molecules were arranged along the y axis.

At various locations on the CO lattice, tunneling spectroscopy was performed. Spectra measured just above the molecule or at the midpoint between two molecules did not show any position dependence. However, spectra acquired at the centers of CO triangles varied depending on the locations [Figs. 4(a) and 4(b)]. It is obvious that the spectra can be categorized in two groups. One group has only a large main peak [marked with filled circles in Fig. 4(b)], while the other group has two subpeaks on either side of the main peak [marked with filled triangles in Fig. 4(b)]. Furthermore, the main peak appears at slightly higher energy if it is accompanied by the two subpeaks. In Fig. 4(a), the spectroscopy locations are indicated with open triangles

having two opposite orientations for the two different sets of spectra. Since p elements are strongly repulsive scatterers of electrons [32], adsorbed CO molecules increase the potential energy of the surface-state electrons in their vicinity, and force them into the honeycomb-shaped region between them [see the inset of Fig. 4(a)]. The locations indicated by the triangles correspond to two equivalent triangular sublattices A and B of the honeycomb. Thus, the spectroscopy directly indicates that LDOS(A) differs from LDOS(B), and that the equivalence of the sublattice degree of freedom of the wave functions is lost in the (8×8) structure. Because the symmetries of the Cu(111) lattice and the CO superstructure are both threefold, this experimental result cannot be understood intuitively.

Another (8×8) structure composed of 19 CO molecules was formed into a hexagonal shape that had better symmetry than that above [Fig. 5(a)]. The detailed shapes of spectra in Fig. 5(b) are different from those in Fig. 4(b), but there is again sublattice dependence. The same large feature reflecting the Shockley state is observed, while the subpeaks appear at different positions relative to those in Fig. 4(b). These subpeaks can be attributed to resonance states at the apex of the tip [26], which probably originated from Cu clusters transferred from the substrate. They appeared reproducibly as long as the tip condition was maintained, but changed if the tip was poked into the surface.

To exclude the tip effect and to clarify the perturbation given by the CO lattice to the 2DEG, we normalized the spectra [Figs. 6(a)–6(d)] with a background spectrum established by averaging two spectra obtained at locations outside the lattice [1 and 8 in Fig. 6(b)]. In Fig. 6(c), the background
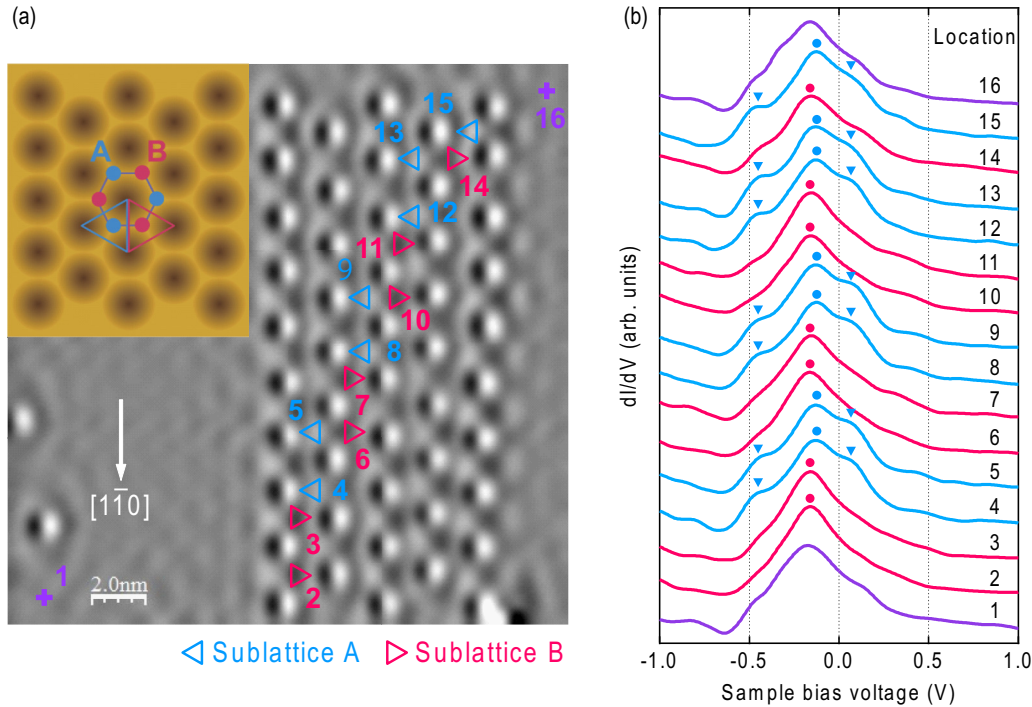
FIG. 4. Tunneling spectroscopy on an (8×8) CO structure formed on Cu(111). (a) Spectroscopy locations are indicated by open triangles with opposite orientations that correspond to A and B sublattice sites of a honeycomb lattice. The inset at upper left is a schematic of molecular graphene. Note that the honeycomb lattice sites correspond to centers of CO triangles, and the configuration of the CO triangle depends on the sublattice (A or B). (b) Tunneling spectra measured at numbered locations indicated in the image. The set point was $V_b = -1.0$ V, $I = 6.0$ nA, and the modulation for lock-in detection was $V_{AC} = 15$ mV, $f = 277$ Hz. Spectra 2–16 are offset vertically for clarity. Positions of the main peaks and subpeaks are marked with filled circles and triangles. Spectra obtained for sublattice A show the main peaks at higher energy than those obtained for sublattice B. The subpeaks appear only in the spectra for sublattice A.

was subtracted from all the spectra, whereas, in Fig. 6(d), all the spectra were divided by it. Both actions revealed basically the same spectral features. Quantitatively, division is the correct method, but tends to enhance the peaks at higher energies. Because we are most interested in energies near E_F, the subtraction normalization method was preferred in the following qualitative discussions. As shown in Fig. 6(c), the characteristic features near E_F had significant sublattice dependence. The spectra associated with sublattice A decreased at E_F with an enhanced peak at about $V_b = -0.1$ V, while the spectra associated with sublattice B slightly increased at E_F without a large peak.

All the normalized spectra exhibited dips at around $V_b = -0.35$ V. The same dips were observed for spectra obtained for a one-dimensional (1D) periodic CO structure as shown in Figs. 7(a) and 7(b). Therefore, this feature is not related to the threefold symmetry of the CO lattice, but rather to the CO molecules themselves. On the Cu(111) plane, surface-state electrons form the 2DEG confined between the L gap and the vacuum and are thus completely decoupled from the bulk. These electrons are scattered by the CO molecules in three ways (see inset of Fig. 8): reflected to the surface state on the same side as the incidence (reflection); transmitted across the molecules into the surface state on the other side (transmission); and absorbed into the bulk states (absorption). Therefore, in the presence of adsorbed CO molecules, the surface state is coupled to the bulk by absorption, resulting in a surface resonance with a finite lifetime [32]. The effect of

this process should appear in tunneling spectra as lifetime broadening and DOS reduction of the surface-state band bottom. This was confirmed in the tunneling spectra (Fig. 8), and was observed as the dips in the normalized spectra [Figs. 6(c) and 7(b)].

Hörmandinger and Pendry [32] obtained band structures of Cu(111) surfaces with (6×2) structures of adsorbed atoms by using a layer-Korringa-Kohn-Rostoker (LKKR) formalism. They examined the properties of single rows of scatterers by fitting a 1D model which assumed complex potential barriers or wells to simulate the coupling of the surface state to the bulk. They found that p elements like C and S are repulsive scatterers and have higher absorption probabilities relative to d elements such as Fe and Cu. Adjusting the parameters of the model to reproduce the LKKR band structures, they estimated the probability of the absorption into the bulk at 0.52 for C and S, 0.25 for Fe, and 0.19 for Cu. For Fe adsorbed on Cu(111), Heller $et~al.$ used a theory where electron scattering by an adatom is parametrized by a complex scattering phase shift [33]. They fit the model to the standing-wave patterns observed by STM, and determined that the imaginary part of the phase shift was infinity, concluding that the Fe adatoms had the "black dot" behavior with maximal attenuation. The absorption probability was estimated at 0.5 for an infinite line of Fe atoms spaced by four Cu lattice sites. For the (8×8) CO structure here, the CO molecules are repulsive scatterers, and Bragg scattering has more channels into the bulk than into the surface state [32]. Hence, the probability of the
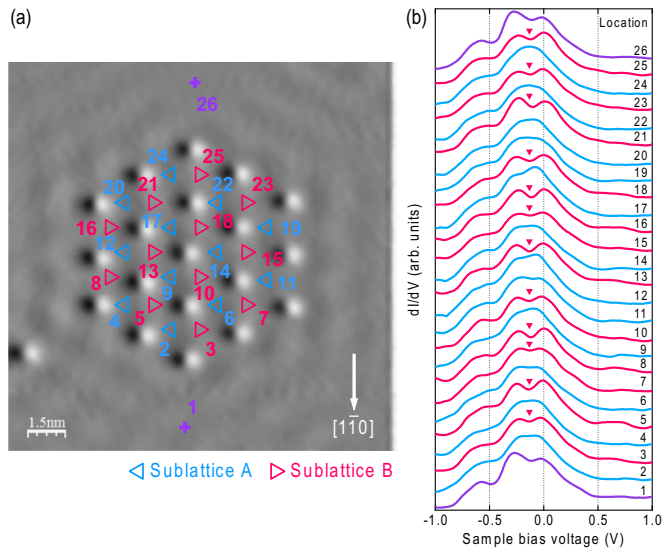
FIG. 5. Tunneling spectroscopy on an (8×8) structure of 19 CO molecules on Cu(111) in a hexagonal shape. (a) STM image (derivative display) indicating spectroscopy locations. The imaging conditions were $V_b = -0.1$ V, $I = 0.2$ nA, 15×15 nm^2, $T = 7.2$ K. (b) Tunneling spectra measured at the A and B sublattice sites. The set point was $V_b = -1.0$ V, $I = 10.0$ nA, and the modulation for lock-in detection was $V_{AC} = 15$ mV, $f = 277$ Hz. Spectra 2–26 are offset vertically for clarity. Spectra obtained for sublattice B have dips (marked with filled triangles) below E_F; spectra for sublattice A do not have. Subpeaks, observed at all locations including ones away from the CO lattice (spectra 1 and 26), can be attributed to resonance states originating from Cu clusters picked up by the W tip.

absorption is expected to be high relative to the other scattering processes.

To clarify how the LDOS varies in real space, STS was performed [Figs. 9(a)–9(d)]. Figure 9(b) is an STS image with $V_b = -0.1$ V that was acquired simultaneously with the STM image in Fig. 9(a). The CO molecules in Fig. 9(b) appear as dark spots, and triangles formed by them show contrast roughly in the same scale as the CO lattice. The bright (dark) areas correspond to the A (B) sublattice sites. Figure 9(c) plots averages of the normalized spectra acquired at the A and B sublattice sites shown in Fig. 6(c). Considering that the enhanced peak at about $V_b = -0.1$ V was observed only at the A sublattice sites, the STS image contrast is consistent with the spectroscopy. For $V_b = -0.02$ V, the contrast disappeared [Fig. 9(d)], as can be expected from Fig. 9(c).

The origin of the sublattice site dependence of the LDOS can be attributed to the second layer of Cu(111), as illustrated in Fig. 9(e) where the second layer appears as open circles. Both A and B sublattice sites are hollow sites on the topmost layer and are equivalent (Fig. 1). However, the A and B sublattice sites are nonequivalent on-top and hollow sites in the second layer, respectively [Fig. 9(e)]. Hence, the second layer appears to induce the LDOS variation. Tunneling spectra measured at various locations on the clean Cu(111) surface, however, basically have the same features with no LDOS site dependence. Therefore, it is likely that the CO molecules strengthen the coupling between the surface state and the bulk via the absorption process, and enhance effects of the second layer.

Since the CO molecules only weakly undulate the STM and STS images, the CO lattice yields a shallow periodic potential having minima at the sublattice sites where the relative positions of the second layer Cu are different depending on
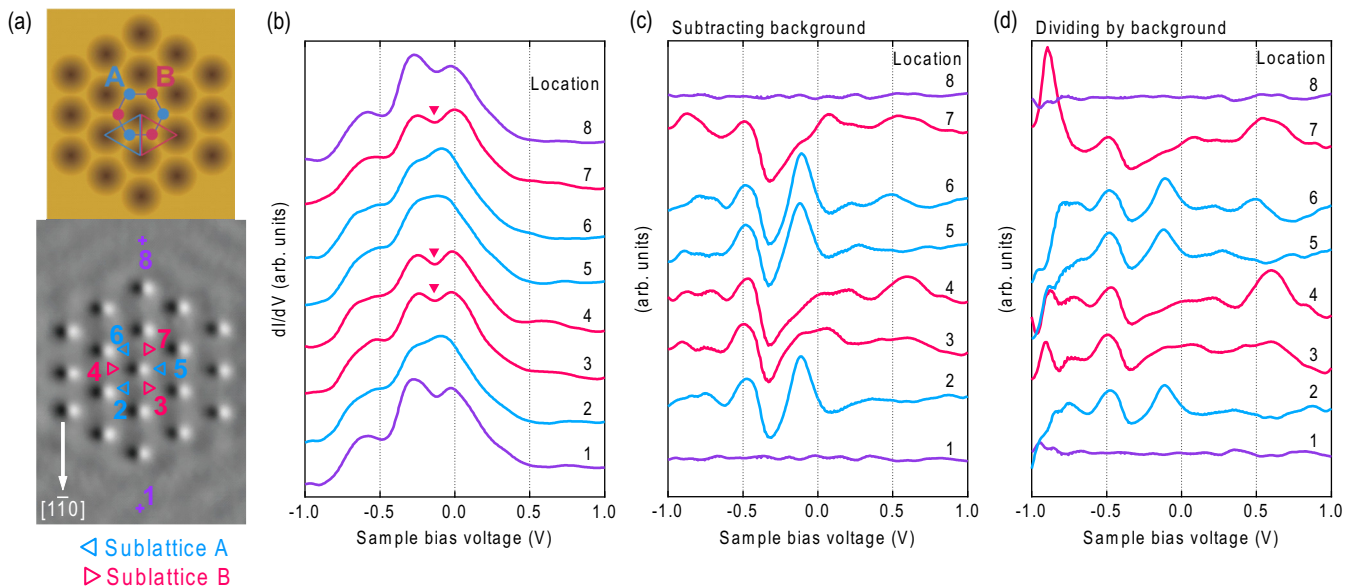
FIG. 6. Normalization of tunneling spectra to exclude the tip effect. (a) Schematic and STM image (derivative display) of the (8×8) CO structure indicating spectroscopy locations. (b) Tunneling spectra measured at the A and B sublattice sites. Spectra 2–8 are offset vertically for clarity. (c) Normalized spectra obtained by subtracting a background spectrum that is an average of spectra 1 and 8, both measured at the locations away from the CO lattice. The observed sublattice site dependence originates from features in the range $|V_b| < 0.15$ V. (d) Normalized spectra obtained by dividing original spectra by the background spectrum. The same tendency as (c) is observed, except for the enhancement of spectral features at higher bias voltages.
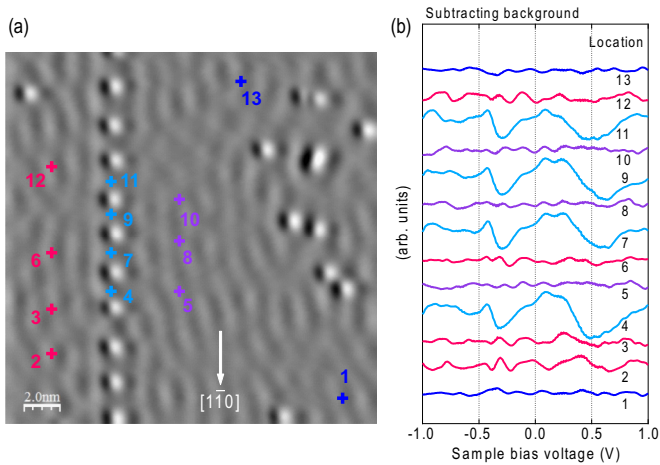
FIG. 7. Tunneling spectroscopy on a 1D CO structure on Cu(111). (a) STM image (derivative display) obtained with the imaging conditions $V_b = -0.01$ V, $I = 1.0$ nA, 20×20 nm^2, $T = 7.8$ K. The CO molecules were periodically arranged with a spacing of 20.4 Å. Spectroscopy locations are indicated by numbered marks. (b) Tunneling spectra normalized by subtracting a background spectrum obtained by averaging spectra 1 and 13 measured at locations away from the 1D structure. The set point was $V_b = -1.0$ V, $I = 4.0$ nA, and the modulation for lock-in detection was $V_{AC} = 15$ mV, $f = 277$ Hz. Spectra 2–13 are offset vertically for clarity. Spectra measured at locations near the CO molecules had dips at about $V_b = -0.35$ V.

the sublattice (A or B). In Fig. 9(e), two large circles with diameters three times the Cu(111) lattice are superimposed at the A and B sublattice sites. The arrangements of second-layer Cu inside the circles are quite different. Because the spatial variation of the LDOS occurs on a scale larger than the Cu(111) lattice, the second-layer Cu atoms near the potential minima must work collectively to produce a difference in the crystal field and, thus, the minimum potential energy. This would affect LDOS(A) and LDOS(B) differently. Figure 9(f) schematically illustrates the cross section and the expected potential energy for the surface-state electrons plotted along the dashed line indicated in Fig. 9(e).

To support this conclusion, first-principles calculations for LDOS of a CO superstructure on Cu(111) were performed. They were based on the nonequilibrium Green's-function method combined with DFT [33], and used a (4 × 4) structure which has the same relative positions between the A and B sublattice sites and the second-layer Cu atoms. A Cu (111) slab for the simulation model is illustrated in Figs. 10(a) (side view) and 10(b) (top view). The model structure is an array of Cu (111) slabs, each with six layers and with adsorbed CO molecules on one surface. 15-Å-thick vacuum spaces separate the slabs to cut off interactions between them along the z direction. The central region of the slab is 1.0225×7.0838 nm^2 in the x-y plane, and has the (4 × 4) CO structure. It is connected to two semi-infinite electrical leads, i.e., clean Cu(111), on both sides in the y direction. A periodic boundary condition was applied only in the x direction. The LDOS at the surface was obtained by averaging over the 1.28-Å-thick surface region [shaded in Fig. 10(a)].
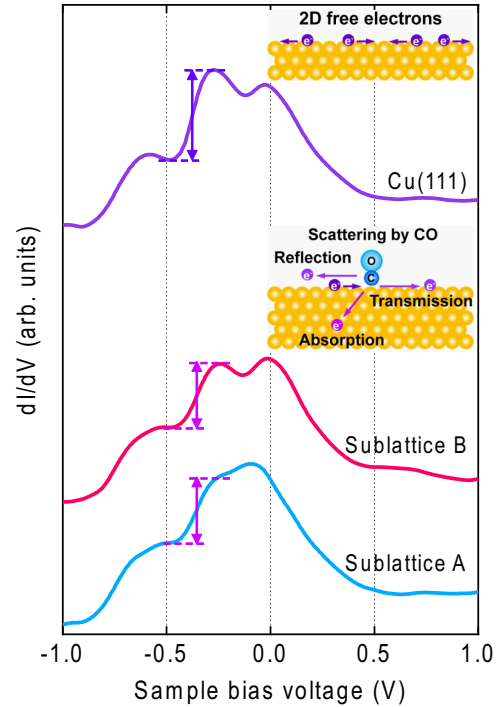
FIG. 8. Scattering of surface-state electrons by an adsorbed CO molecule on Cu(111). Nearly free 2D electrons are scattered by the CO molecule in three ways: reflection, transmission, and absorption (insets). Averages of tunneling spectra obtained for sublattice A, sublattice B, and the bare Cu(111) surface [form Fig. 6(b)], are plotted for comparison. Note that the increases in differential conductance at $V_b = -0.4$ V for sublattices A and B are smaller than that measured for the bare Cu(111). This indicates lifetime broadening and reduction of the surface state DOS due to the absorption process, which appears as dips at about $V_b = -0.35$ V in the normalized spectra.

In the "CO-adsorption puzzle," DFT based on the local-density approximation (LDA) or GGA description fails to predict the correct adsorption site for CO on metal surfaces [34]. On Cu(111), the fcc hollow site is preferred if the standard LDA and GGA functionals are used, although, experimentally, the on-top site is the most stable. This is because calculations using LDA and GGA functionals underestimate the gap between the highest occupied molecular orbital (HOMO) and the lowest unoccupied molecular orbital (LUMO) of CO on Cu(111), and thus overestimate the hybridization between the CO orbitals and the Cu states, which prefers the higher-coordination sites. This problem has been solved by using hybrid functionals that combine exact nonlocal orbital-dependent Hartree-Fock exchange and a standard local exchange-correlation functional [29,30]. Here, however, the LDOS was calculated using the PBE-GGA functional assuming that the CO molecules occupied on-top sites. It was expected that this method would yield useful information regarding electronic states near E_F, where the HOMO and the LUMO positions do not strongly affect the results.

Figures 10(c) and 10(d) demonstrate the calculated LDOS of the Cu(111) surface with and without CO molecules at an energy -0.1 eV below E_F, which equals the bias voltage used
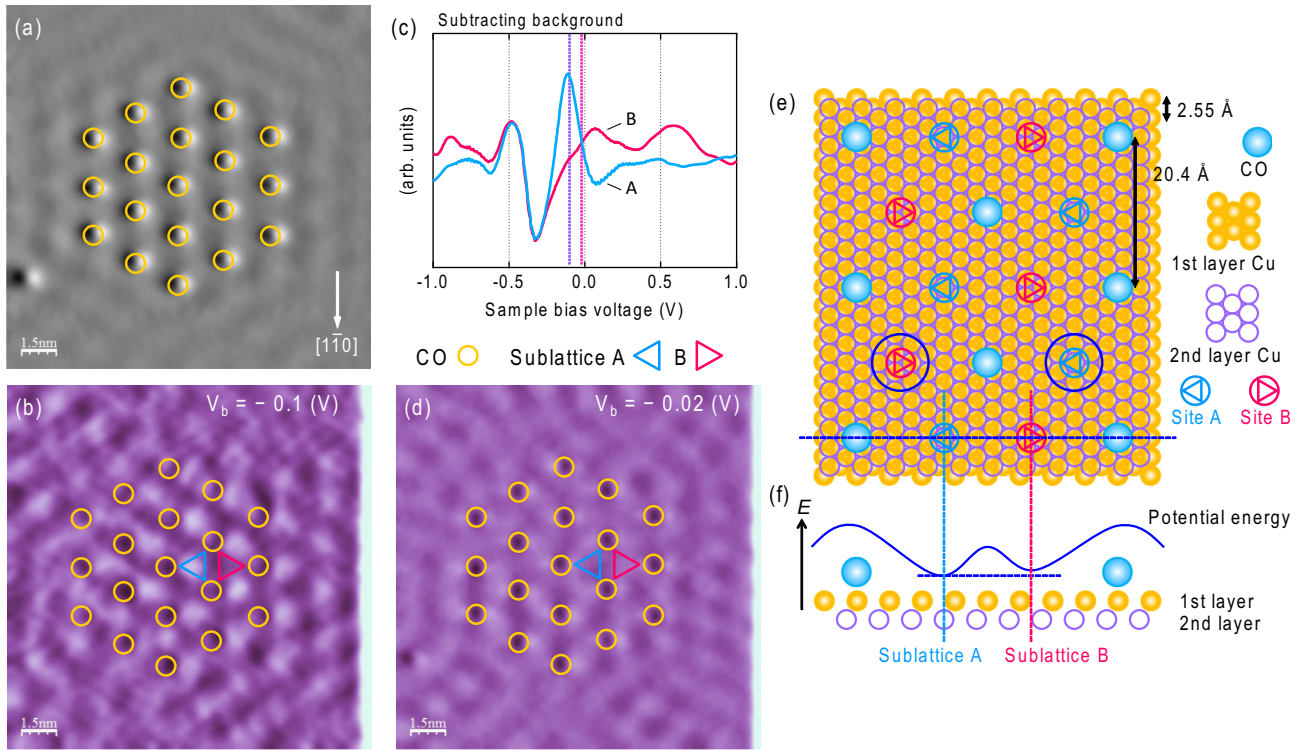
FIG. 9. STS observations on the (8×8) structure of 19 CO molecules on Cu(111) in a hexagonal shape. (a) STM image (derivative display) obtained with $V_b = -0.1$ V, $I = 1.0$ nA, 15×15 nm^2, $T = 7.2$ K. Locations of adsorbed CO molecules are marked with open circles. (b) STS image simultaneously obtained (contour display). The modulation for lock-in detection was $V_{AC} = 10$ mV, $f = 277$ Hz. A bright (dark) area corresponding to the A (B) sublattice site is marked with an open triangle. (c) Averages of normalized spectra for sublattices A and B obtained by subtraction of the background [from Fig. 6(c)]. The bias voltages for the STS are indicated by dotted lines. (d) STS image (contour display) measured at the same location. The imaging conditions were $V_b = -0.02$ V, $I = 0.3$ nA, 15×15 nm^2, $T = 7.2$ K, and the modulation was $V_{AC} = 10$ mV, $f = 277$ Hz. The contrast between the A and B sublattice sites disappeared. (e) Schematic of the (8×8) CO structure. The second layer of Cu(111) is superimposed (open circles) showing that the sublattices A and B are not equivalent if it is taken into account. (f) Schematic of the cross section and the potential for surface-state electrons along the dashed line indicated in (e).

for the STS imaging [Fig. 9(b)]. The maps are displayed in a logarithmic scale. The triangular lattice corresponds to Cu atoms in the topmost layer. The small dots appearing to the right of them correspond to locations of the second-layer Cu atoms. In Fig. 10(c), large open circles show the positions of the (4×4) CO structure, and large open triangles indicate the (4×4) lattice with centers that correspond to the A and B sublattice sites. The same locations on the clean surface
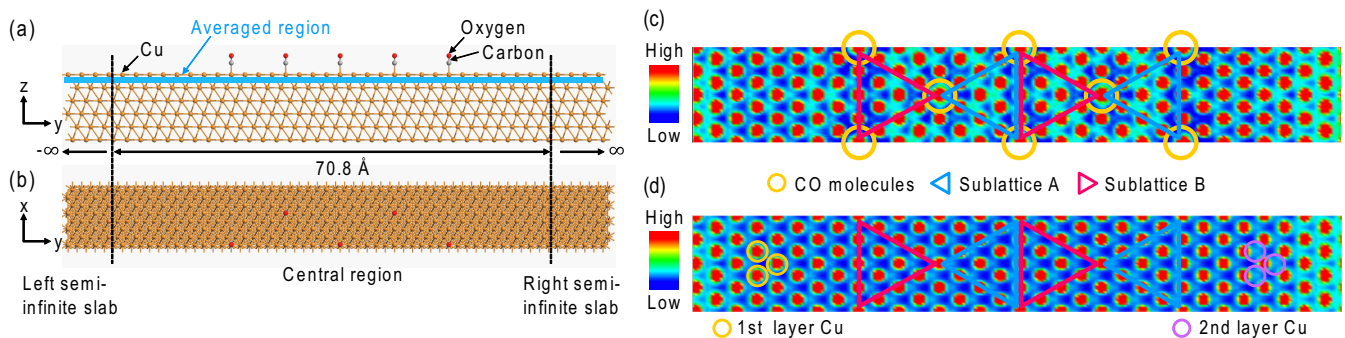
FIG. 10. Simulation model for calculated LDOS of a (4×4) CO structure on Cu(111). (a) Side view of the simulation model, where the central region is a Cu (111) slab with six layers and a (4×4) CO structure on one surface. Cu-Cu, Cu-C, and C-O distances are 2.56, 1.88, and 1.16 Å, respectively. The central region is connected to two clean Cu (111) slabs on both sides in the y direction. A periodic boundary condition is adopted in the x direction. (b) Top view of the simulation model. (c) LDOS of the simulation model calculated for the energy -0.1 eV below E_F, which equals the bias voltage for the STS image [Fig. 9(b)]. The LDOS is averaged over a 1.28-Å-thick surface region [shaded area in (a)]. The open triangles indicate the (4×4) CO triangular lattice whose centers correspond to A and B sublattice sites of molecular graphene, and whose corners are all occupied by CO molecules (open circles). The LDOS map is displayed in a logarithmic scale. (d) LDOS of a clean surface of the six-layered Cu(111) slab calculated in the same manner.
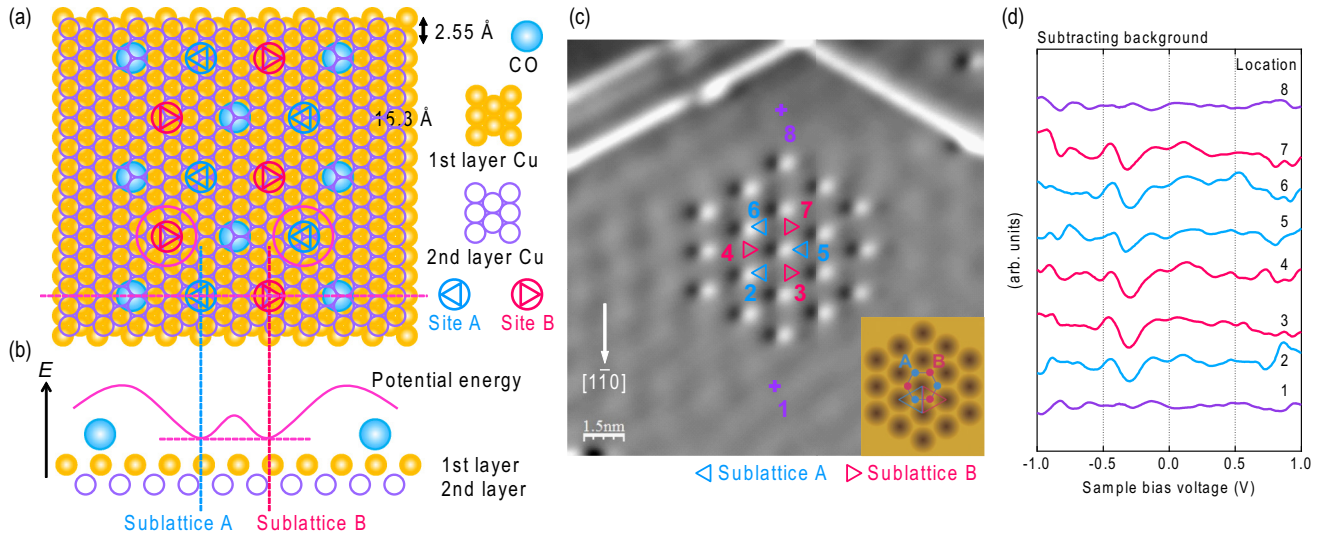
FIG. 11. A (6×6) structure of 19 CO molecules on Cu(111) in a hexagonal shape. (a) Schematic of a (6×6) CO structure on Cu(111). A and B sublattice sites are equivalent on both the first and second layers of Cu(111). (b) Schematic of the cross section and the potential for surface-state electrons along the dashed line indicated in (a). (c) STM image of a (6×6) CO structure on Cu(111). Spectroscopy locations corresponding to A and B sublattice sites are indicated by open triangles. The imaging conditions were $V_b = -0.2$ V, $I = 0.2$ nA, 15×15 nm^2, $T = 5.7$ K. (d) Tunneling spectra measured at the locations indicated in the image. All the spectra were normalized by subtracting the background that was an average of spectra 1 and 8. The set point was $V_b = -1.0$ V, $I = 10.0$ nA, and the modulation for lock-in detection was $V_{AC} = 10$ mV, $f = 277$ Hz. Spectra 2–8 are offset vertically for clarity. Sublattice site dependence of the spectrum was not observed.

are marked in Fig. 10(d). In the LDOS maps, LDOS(A) is higher than LDOS(B). This difference was very weak on the clean surface [Fig. 10(d)], which was probably undetectable by STM/STS, but was enhanced by the CO lattice [Fig. 10(c)]. This sublattice site dependence was not reported previously for the same model surface using a similar calculation method [35].

Although the calculations here reproduced the sublattice site dependence, the detailed features of the LDOS spatial variation were different from those in the STS data. In the calculated LDOS, Cu atoms in the topmost layer were clearly shown, but they were not resolved in the STM/STS experiments. This was probably because the Cu $4sp_z$ orbital dominates the STM tunneling [24], while the calculated LDOS accumulates all of the Cu $3d$, $4s$, and $4p$ orbitals.

The above effects of the A and B sublattice sites should not be observed if their lattice sites are equivalent on both the first and second Cu(111) layers. This should be the case for a $(N \times N)$ CO structure where $N = 3n$ $(n = 1, 2, 3 \ldots)$. Figure 11(a) is a schematic of a (6×6) structure $(n = 2)$, where the potential minima located at both sublattice sites must be even [Fig. 11(b)]. Tunneling spectroscopy was performed on a fabricated (6×6) CO structure [Figs. 11(c) and 11(d)], and all the spectra acquired on the CO lattice had dips at around $V_b = -0.35$ V due to the absorption process of surface-state electrons, but did not exhibit sublattice site dependence. This confirmed the above conclusions.

Gomes *et al.* fabricated "molecular graphene" composed of hundreds of CO molecules [18]. Tunneling spectroscopy revealed a decrease in the DOS near E_F accompanied with enhanced peaks at about $V_b = \pm 0.1$ V, which indicated Dirac cones and the Van Hove singularity of the graphenelike electronic structure. Here, such features were not observed in

tunneling spectra. Aichinger *et al.* examined single-electron properties of artificial graphene flakes with a model potential consisting of circular scattering centers positioned in a triangular lattice surrounded by a hexagonal boundary [36]. They revealed gradual formation of Dirac cones as the flake size increased; the cones were more pronounced with 61 scattering centers. The superstructures here were formed by only 19 or 48 CO molecules; it is possible that Dirac cones might have emerged if the number had been greater.

In contrast, we observed the sublattice site dependence of the LDOS in the smallest molecular graphene flake of seven CO molecules. The change in DOS due to this effect can be estimated at 10–15% of the total DOS, whereas there was a 30–40% variation derived from the Dirac cones observed for molecular graphene [18]. If the same phenomenon occurs in molecular graphene, the equivalence of electronic structures near the K and K' points in the hexagonal Brillouin zone would be lost, which breaks the sixfold symmetry of the graphenelike electronic structure. Consequently, the results here suggest that the symmetry of the pseudospin states of the molecular graphene in the $(N \times N)$ configuration, where $N = 3n \pm 1$, originally breaks without any external perturbation such as distortion [37,38] or a pseudomagnetic field [39–41]. This situation is similar to the terminating layer of graphite with Bernal–type stacking [42,43], and to monolayer graphene epitaxially grown on Cu(111) or SiC [44,45] with good lattice matching, where inequivalent potentials on the sublattices are induced by the interface. Although artificial graphene attracts interest in the fabrication of designable Dirac materials, this observed effect must be taken into account, and the periodicity of the external potential should be determined carefully to obtain a tailored electronic structure close to the design.

IV. CONCLUSIONS

Artificial electronic states were created by introducing a periodic potential to the surface state, which was achieved by manipulating CO molecules into superstructures on a Cu(111) surface with LT-STM. Local electronic states on two equivalent triangular sublattices were inequivalent on a (8×8) structure but equivalent on a (6×6) structure. First-principles calculations for the LDOS reproduced the sublattice site dependence for a (4×4) structure. This dependence was understandable in terms of the external periodic potential that was perturbed by the second layer of Cu(111), which was enhanced by absorption of the surface state electrons into the bulk. It is expected that the symmetry of the pseudospin states of molecular graphene in the $(N \times N)$ configuration will be broken when $N = 3n \pm 1$ ($n = 1, 2, 3 \ldots$), but conserved when $N = 3n$ without any external perturbation. These results suggest that translational symmetry breaking at the surface in the normal direction affects an artificial 2D electron system through scattering, which is governed by the lattice spacing of the adsorbates forming the superstructure.

[1] A. Zangwill, *Physics at Surfaces* (Cambridge, New York, 1988).

[2] S. G. Davison and M. Stęślicka, *Basic Theory of Surface States* (Oxford, New York, 1992).

[3] F. Reinert, G. Nicolay, S. Schmidt, D. Ehm, and S. Hüfner, Phys. Rev. B **63**, 115415 (2001).

[4] M. F. Crommie, C. P. Lutz, and D. M. Eigler, Nature (London) **363**, 524 (1993).

[5] D. M. Eigler and E. K. Schweizer, Nature (London) **344**, 524 (1990).

[6] M. F. Crommie, C. P. Lutz, and D. M. Eigler, Science **262**, 218 (1993).

[7] C. R. Moon, L. S. Mattos, B. K. Foster, G. Zeltzer, W. Ko, and H. C. Manoharan, Science **319**, 782 (2008).

[8] H. C. Manoharan, C. P. Lutz, and D. M. Eigler, Nature (London) **403**, 512 (2000).

[9] M. Z. Hasan and C. L. Kane, Rev. Mod. Phys. **82**, 3045 (2010).

[10] A. H. Castro Neto, F. Guinea, N. M. R. Peres, K. S. Novoselov, and A. K. Geim, Rev. Mod. Phys. **81**, 109 (2009).

[11] C.-H. Park and S. G. Louie, Nano Lett. **9**, 1793 (2009).

[12] E. Räsänen, C. A. Rozzi, S. Pittalis, and G. Vignale, Phys. Rev. Lett. **108**, 246803 (2012).

[13] E. Kalesaki, C. Delerue, C. Morais Smith, W. Beugeling, G. Allan, and D. Vanmaekelbergh, Phys. Rev. X **4**, 011010 (2014).

[14] M. Gibertini, A. Singha, V. Pellegrini, M. Polini, G. Vignale, A. Pinczuk, L. N. Pfeiffer, and K. W. West, Phys. Rev. B **79**, 241406(R) (2009).

[15] A. Singha, M. Gibertini, B. Karmakar, S. Yuan, M. Polini, G. Vignale, M. I. Katsnelson, A. Pinczuk, L. N. Pfeiffer, K. W. West, and V. Pellegrini, Science **332**, 1176 (2011).

[16] J. Lobo-Checa, M. Matena, K. Müller, J. H. Dil, F. Meier, L. H. Gade, T. A. Jung, and M. Stöhr, Science **325**, 300 (2009).

[17] S. Wang, W. Wang, L. Z. Tan, X. G. Li, Z. Shi, G. Kuang, P. N. Liu, S. G. Louie, and N. Lin, Phys. Rev. B **88**, 245430 (2013).

[18] K. K. Gomes, W. Mar, W. Ko, F. Guinea, and H. C. Manoharan, Nature (London) **483**, 306 (2012).

[19] I. Horcas, R. Fernández, J. M. Gómez-Rodríguez, J. Colchero, J. Gómez-Herrero, and A. M. Baro, Rev. Sci. Instrum. **78**, 013705 (2007).

[20] K. Stokbro, A. Blom, and S. Smidstrup, in *Proceedings of 18th International Conference on Simulation of Semiconductor Processes and Devices (SISPAD)* (IEEE, New York, 2013).

[21] M. Feng, P. Cabrera-Sanfelix, C. Lin, A. Arnau, D. Sánchez-Portal, J. Zhao, P. M. Echenique, and H. Petek, ACS Nano **5**, 8877 (2011).

[22] L. Bartels, G. Meyer, and K.-H. Rieder, Appl. Phys. Lett. **71**, 213 (1997).

[23] J. A. Nieminen, E. Niemi, and K.-H. Rieder, Surf. Sci. Lett. **552**, L47 (2004).

[24] R. K. Tiwari, D. M. Otálvaro, C. Joachim, and M. Saeys, Surf. Sci. **603**, 3286 (2009).

[25] T. Hofmann, F. Pielmeier, and F. J. Giessibl, Phys. Rev. Lett. **112**, 066101 (2014).

[26] G. Hörmandinger, Phys. Rev. B **49**, 13897 (1994).

[27] G. Blyholder, J. Phys. Chem. **68**, 2772 (1964).

[28] B. Hammer, Y. Morikawa, and J. K. Norskov, Phys. Rev. Lett. **76**, 2141 (1996).

[29] M. Neef and K. Doll, Surf. Sci. **600**, 1085 (2006).

[30] A. Stroppa, K. Termentzidis, J. Paier, G. Kresse, and J. Hafner, Phys. Rev. B **76**, 195440 (2007).

[31] X. Ren, P. Rinke, and M. Scheffler, Phys. Rev. B **80**, 045402 (2009).

[32] G. Hörmandinger and J. B. Pendry, Phys. Rev. B **50**, 18607 (1994).

[33] E. J. Heller, M. F. Crommie, C. P. Lutz, and D. M. Eigler, Nature (London) **369**, 464 (1994).

[34] Q. M. Hu, K. Reuter, and M. Scheffler, Phys. Rev. Lett. **98**, 176103 (2007).

[35] M. Ropo, S. Paavilainen, J. Akola, and E. Räsänen, Phys. Rev. B **90**, 241401(R) (2014).

[36] M. Aichinger, S. Janecek, I. Kylänpää, and E. Räsänen, Phys. Rev. B **89**, 235433 (2014).

[37] V. M. Pereira, A. H. Castro Neto, and N. M. R. Peres, Phys. Rev. B **80**, 045401 (2009).

[38] M. Mohr, K. Papagelis, J. Maultzsch, and C. Thomsen, Phys. Rev. B **80**, 205410 (2009).

[39] I. F. Herbut, Phys. Rev. B **78**, 205433 (2008).

[40] F. Guinea, M. I. Katsnelson, and A. K. Geim, Nat. Phys. **6**, 30 (2010).

[41] N. Levy, S. A. Burke, K. L. Meaker, M. Panlasigui, A. Zettl, F. Guinea, A. H. Castro Neto, and M. F. Crommie, Science **329**, 544 (2010).

[42] D. Tománek, S. G. Louie, H. J. Mamin, D. W. Abraham, R. E. Thomson, E. Ganz, and J. Clarke, Phys. Rev. B **35**, 7790 (1987).

[43] F. Guinea, A. H. Castro Neto, and N. M. R. Peres, Phys. Rev. B **73**, 245426 (2006).

[44] S. Y. Zhou, G.-H. Gweon, A. V. Fedorov, P. N. First, W. A. de Heer, D.-H. Lee, F. Guinea, A. H. Castro Neto, and A. Lanzara, Nat. Mater. **6**, 770 (2007).

[45] S. Y. Zhou, D. A. Siegel, A. V. Fedorov, F. El Gabaly, A. K. Schmid, A. H. Castro Neto, D.-H. Lee, and A. Lanzara, Nat. Mater. **7**, 258 (2008).